eLIFE
elifesciences.org

# Figures and figure supplements

Structural basis of nucleoside and nucleoside drug selectivity by concentrative nucleoside transporters

**Zachary Lee Johnson, et al.**

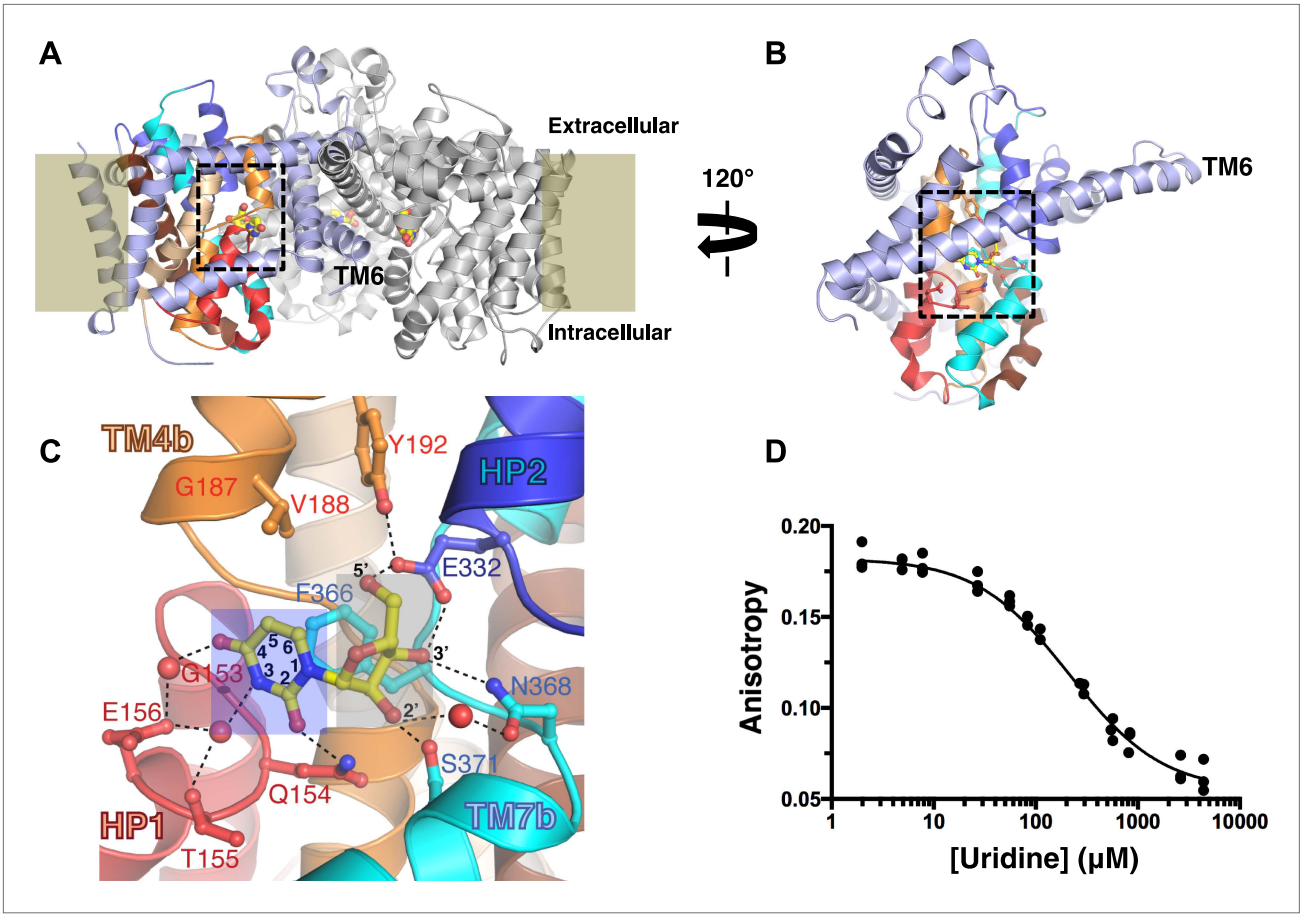


**Figure 1**. The nucleoside-binding site of vcCNT and fluorescence-anisotropy-based competition assay. (**A**) The vcCNT-7C8C trimer viewed from within the plane of the membrane. The location of the membrane is marked by rectangles. The scaffold domain of one protomer is colored light blue, and the transport domain is colored red, blue, orange, cyan, wheat, and brown. The other two protomers are colored gray. Uridine is shown bound to each protomer in stick representation. The nucleoside-binding site is delineated with dashed lines. vcCNT-7C8C functions similarly to wild type (***Figure 1—figure supplement 1***). (**B**) The vcCNT-7C8C protomer. The structure is rotated 120° about the trimer axis relative to **A**, zoomed in, and the other two protomers have been removed for clarity. (**C**) Nucleoside-binding site. Amino acid residues that interact with the uridine are labeled and shown in stick representation and were used for sequence identity calculation with hCNTs. Hydrogen bonds are shown as dashed lines. The uracil base is marked with a blue box, and the ribose is marked with a gray box. For a stereo view of the electron density in the nucleoside-binding site, see ***Figure 1—figure supplement 2***. (**D**) Fluorescence titration of vcCNT with uridine. Uridine was titrated into solution containing vcCNT and the fluorescent nucleoside pyrrolo-cytidine, anisotropy was measured, and data were fit to a single-site competitive binding model to obtain a $K_D$ of 36 ± 3 μM (mean ± SEM, n = 3 measurements).

DOI: 10.7554/eLife.03604.003

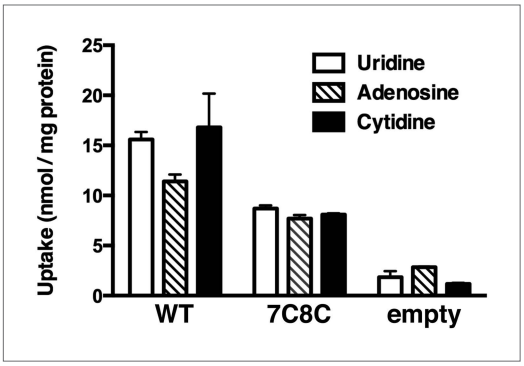


**Figure 1—figure supplement 1**. vcCNT-7C8C maintains nucleoside transport activity. Wild-type (WT) and 7C8C vcCNT were reconstituted into lipid vesicles and assessed for their ability to support the uptake of 2 μM of $^{3}$H-labeled nucleosides as described (***Johnson et al., 2012***). The data shown represent 2 min timepoints. Empty vesicles were included as a negative control.

DOI: 10.7554/eLife.03604.004

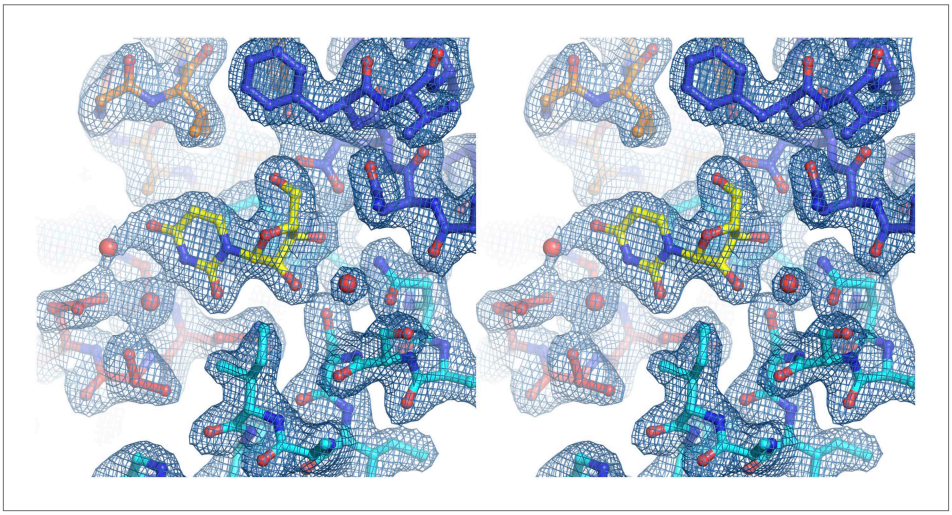

**Figure 1—figure supplement 2**. Electron density at the nucleoside-binding site of vcCNT-7C8C-uridine. The nucleoside-binding site of vcCNT-7C8C bound to uridine is shown in stereo in stick representation in the same orientation and colored as in ***Figure 1C***. Uridine is yellow and the red spheres are water molecules. The resolution is 2.1 Å and density shown is from a $2F_o–F_c$ electron density map contoured at 1σ.

DOI: 10.7554/eLife.03604.005

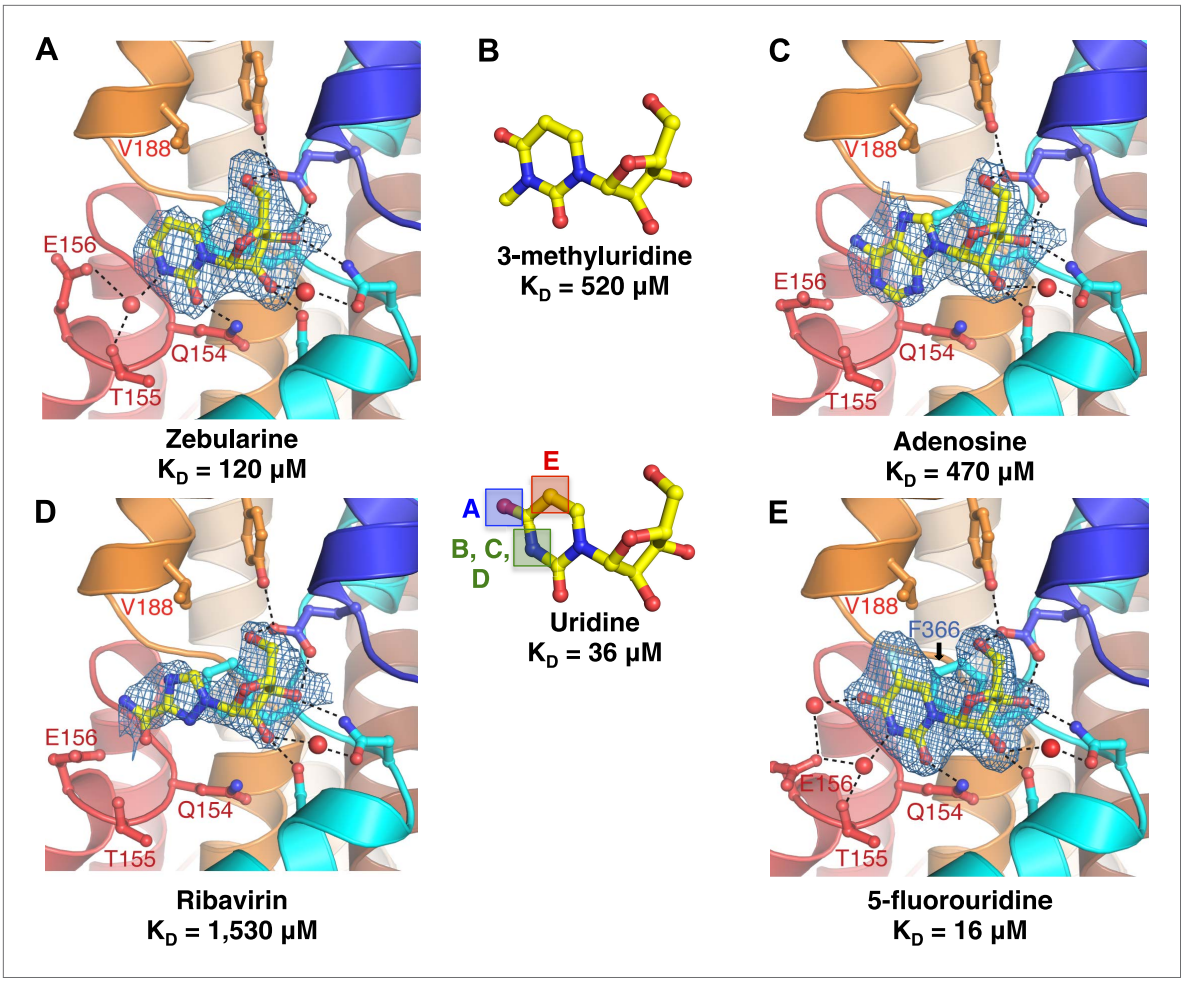


**Figure 2**. Structural basis of nucleobase recognition by vcCNT. (**A**) The crystal structure of vcCNT bound to zebularine. (**B**) Chemical structure of 3-methyluridine. (**C**) The crystal structure of vcCNT-7C8C bound to adenosine. (**D**) The crystal structure of vcCNT-7C8C bound to ribavirin. (**E**) The crystal structure of vcCNT-7C8C bound to 5-fluorouridine. Fluorine is colored cyan. All electron density maps represent $F_o$–$F_c$ SA-OMIT maps for the nucleoside contoured at 3σ. Uridine is shown in the center of the figure for reference. For stereo views of the electron density in the nucleoside-binding site for each of these structures, see ***Figure 2—figure supplements 1–4***.

DOI: 10.7554/eLife.03604.009

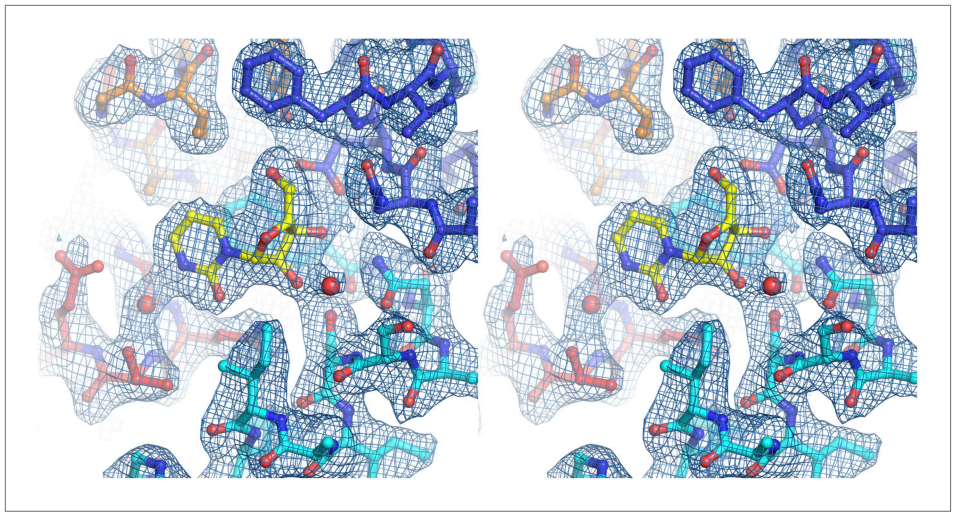

**Figure 2—figure supplement 1**. Electron density at the nucleoside-binding site of vcCNT-zebularine. The nucleoside-binding site of vcCNT bound to zebularine is shown in stereo in stick representation in the same orientation and colored as in ***Figure 2A***. Zebularine is yellow and the red spheres are water molecules. The resolution is 2.9 Å and density shown is from a $2F_o–F_c$ electron density map contoured at 1σ.

DOI: 10.7554/eLife.03604.010

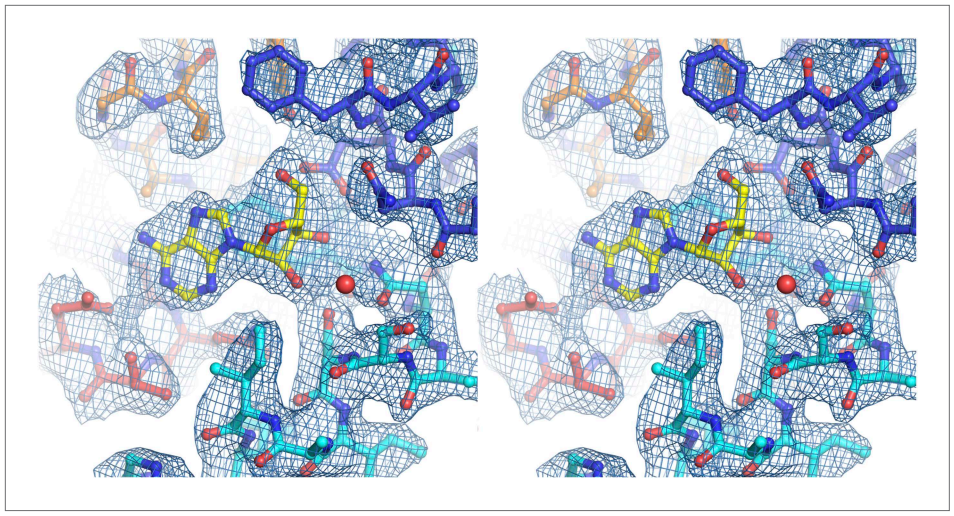

**Figure 2—figure supplement 2**. Electron density at the nucleoside-binding site of vcCNT-7C8C-adenosine. The nucleoside-binding site of vcCNT-7C8C bound to adenosine is shown in stereo in stick representation in the same orientation and colored as in ***Figure 2C***. Adenosine is yellow and the red sphere is a water molecule. The resolution is 3.1 Å and density shown is from a $2F_o–F_c$ electron density map contoured at 1σ.

DOI: 10.7554/eLife.03604.011

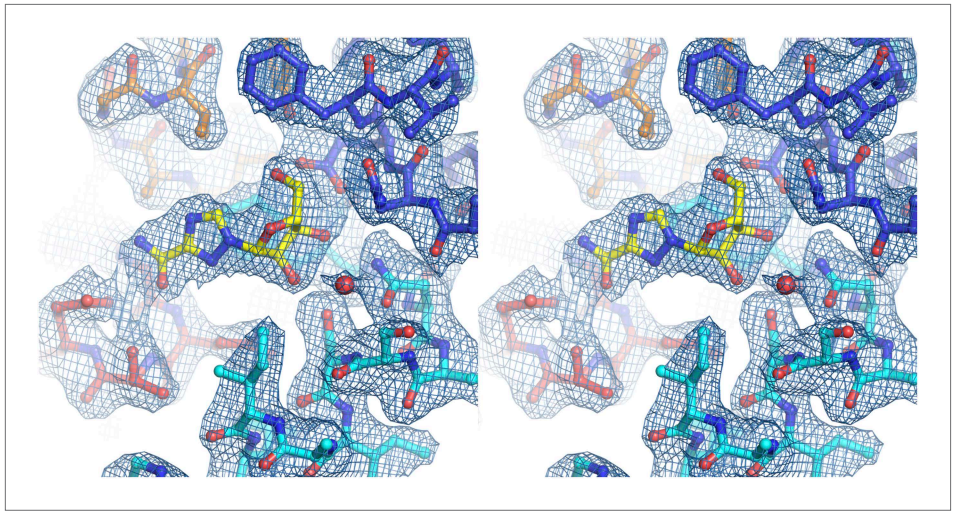

**Figure 2—figure supplement 3**. Electron density at the nucleoside-binding site of vcCNT-7C8C-ribavirin. The nucleoside-binding site of vcCNT-7C8C bound to ribavirin is shown in stereo in stick representation in the same orientation and colored as in ***Figure 2D***. Ribavirin is yellow and the red sphere is a water molecule. The resolution is 2.8 Å and density shown is from a $2F_o–F_c$ electron density map contoured at 1σ.

DOI: 10.7554/eLife.03604.012

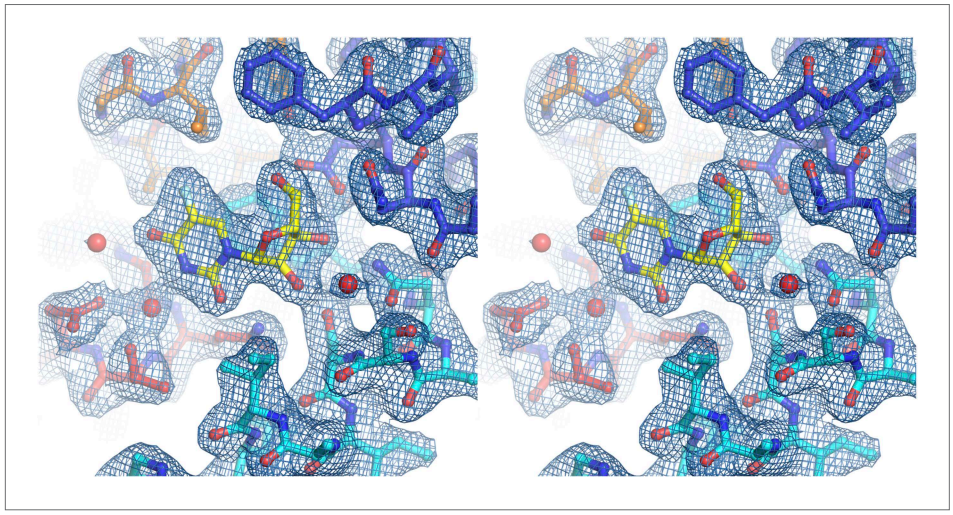

**Figure 2—figure supplement 4**. Electron density at the nucleoside-binding site of vcCNT-7C8C-5-fluorouridine. The nucleoside-binding site of vcCNT-7C8C bound to 5-fluorouridine is shown in stereo in stick representation in the same orientation and colored as in ***Figure 2E***. 5-fluorouridine is yellow and the red spheres are water molecules. The resolution is 2.3 Å and density shown is from a $2F_o–F_c$ electron density map contoured at 1σ.

DOI: 10.7554/eLife.03604.013

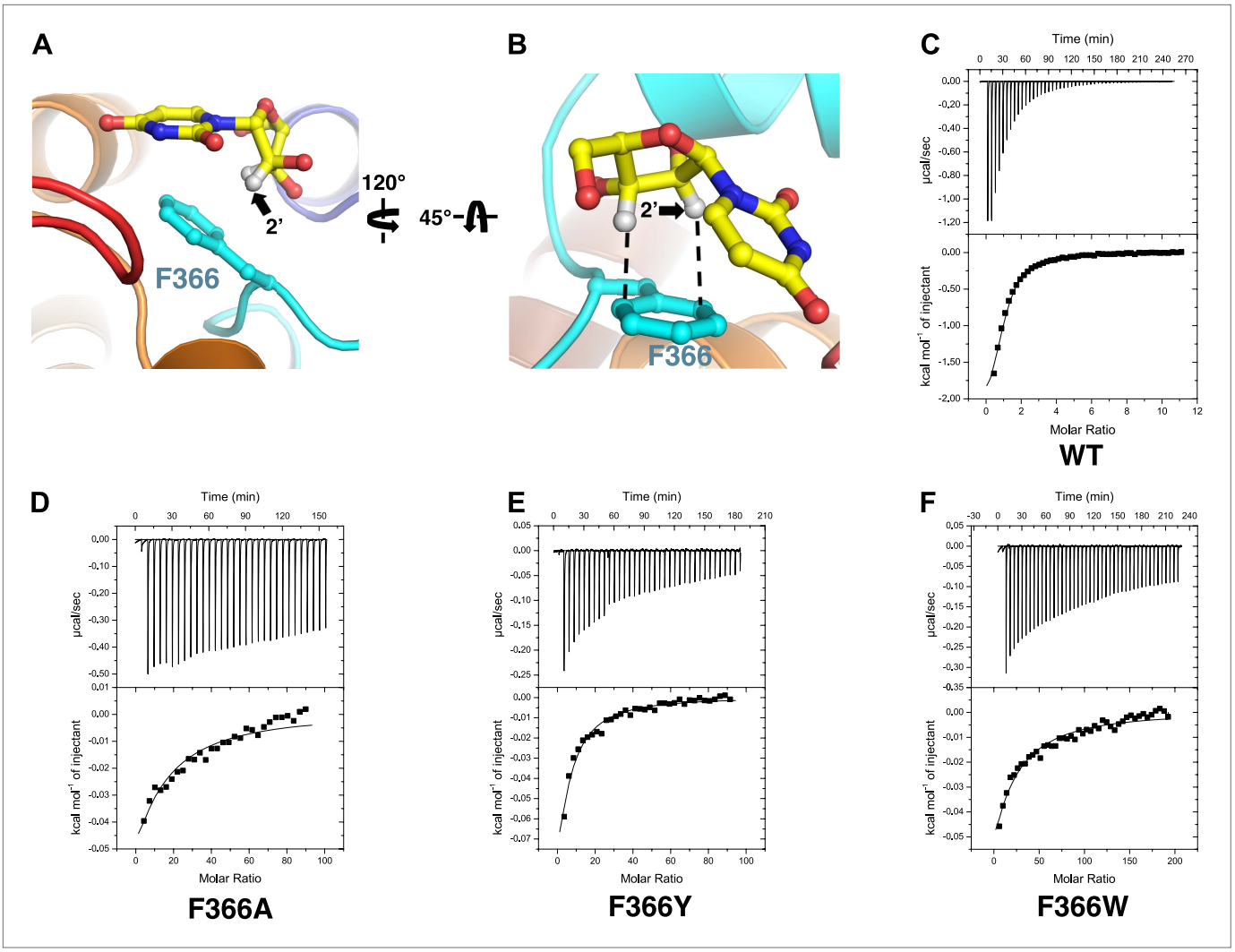


**Figure 3**. Phe 366 is crucial for nucleoside binding by vcCNT. (**A**) The nucleoside-binding site of vcCNT-7C8C bound to uridine is shown viewed from the cytoplasm. Phe 366 interacts with the uracil base via π–π interactions. The other epimeric 2′ position is marked with an arrow. (**B**) Another view of the interaction between Phe 366 and uridine. Phe 366 interacts with the ribose via CH–π interactions (dashed lines). (**C**–**F**) Isothermal titration calorimetry of uridine binding to wild-type vcCNT and Phe 366 mutants. $K_D$ = 45 ± 8 μM and ΔH° = −2970 ± 330 cal/mol for WT, $K_D$ = 1630 ± 120 μM and ΔH° = −2200 ± 190 cal/mol for F366A, $K_D$ = 920 ± 170 μM and ΔH° = −1600 ± 440 cal/mol for F366Y, and $K_D$ = 1470 ± 90 μM and ΔH° = −3190 ± 130 cal/mol for F366W (means ± SEM, n = 3 measurements). Note that the $K_D$ for F366A could not be reliably measured due to the low heat associated with binding. Each of the F366 mutants is biochemically stable as evidenced by a single, sharp peak at the expected trimer size when subjected to size-exclusion chromatography (***Figure 3—figure supplement 1***).

DOI: 10.7554/eLife.03604.015

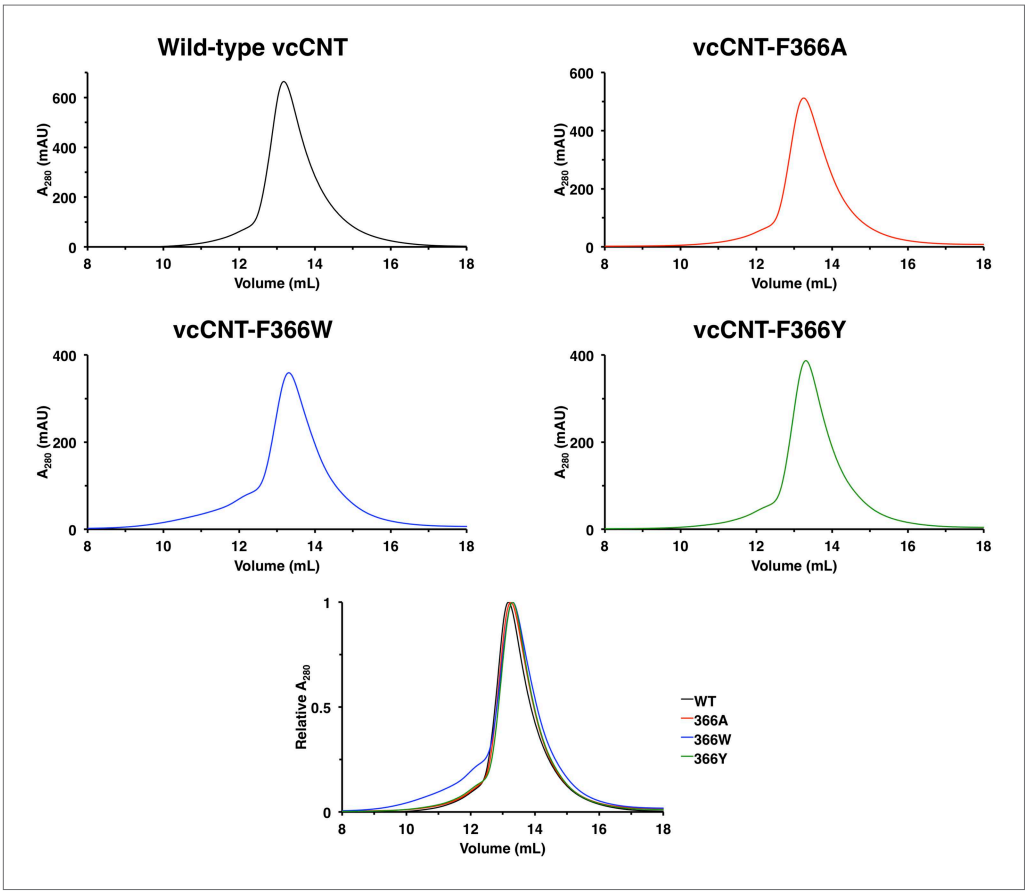


**Figure 3—figure supplement 1**. F366 mutants are biochemically stable. 1 liter of each construct was expressed and purified in parallel without the addition of any exogenous nucleosides as described in the 'Materials and methods'. Each sample was initially purified by size-exclusion chromatography using a Superdex 200 10/300 GL column to remove MBP, and then the peak fractions were collected, concentrated, and re-ran to generate the figures. Each individual chromatogram is shown in the top panels with absolute absorbance at 280 nm on the y-axis, and all of the normalized chromatograms are shown overlaid in the bottom panel.

DOI: 10.7554/eLife.03604.016

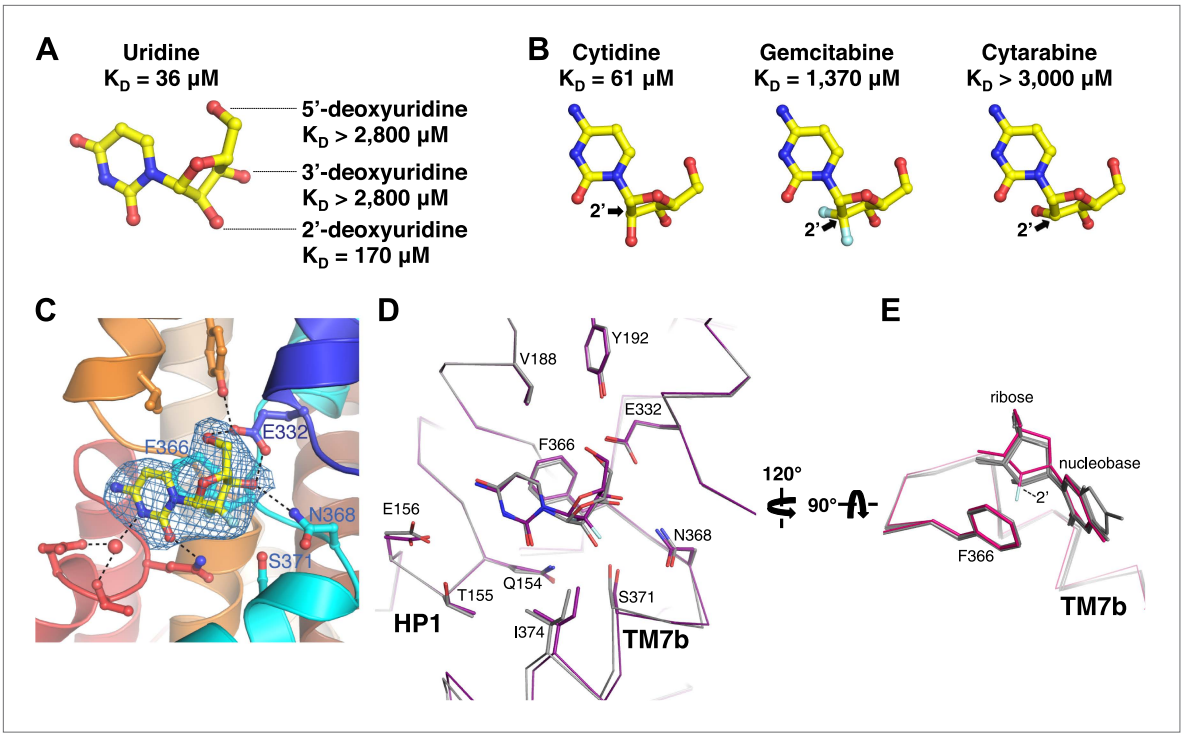


**Figure 4**. Structural basis of ribose recognition by vcCNT. (**A**) Dissociation constants for deoxyuridines. (**B**) Chemical structures and $K_D$s of cytidine, gemcitabine, and cytarabine. The cytidine is from the crystal structure of vcCNT-7C8C bound to cytidine (for a stereo view of the electron density in the nucleoside-binding site of this structure, see ***Figure 4—figure supplement 1***), and the other nucleosides are simply chemical structures in the same orientation as cytidine. Fluorine atoms in gemcitabine are colored cyan. (**C**) Crystal structure of vcCNT-7C8C bound to gemcitabine. Density shown is from an $F_o$–$F_c$ SA-OMIT map contoured at 3σ. For a stereo view of the electron density in the nucleoside-binding site, see ***Figure 4—figure supplement 2***. (**D**) Alignment of uridine-bound and gemcitabine-bound vcCNT structures. Structures were aligned by Cα using PyMOL. TM7 was not used for the alignment. Cα traces and interacting amino acid residues are shown. The uridine-bound vcCNT structure (PDB ID: 3TIJ) is gray and the gemcitabine-bound vcCNT-7C8C structure is deep purple. (**E**) Alignment of vcCNT and vcCNT-7C8C structures bound to uridine (PDB ID: 3TIJ), zebularine, cytidine, pyrrolo-cytidine, 5-fluorouridine, and gemcitabine. Alignments were performed in the same manner as **D**. vcCNT-7C8C-gemcitabine is shown in hot pink and all other structures are shown in gray.

DOI: 10.7554/eLife.03604.017

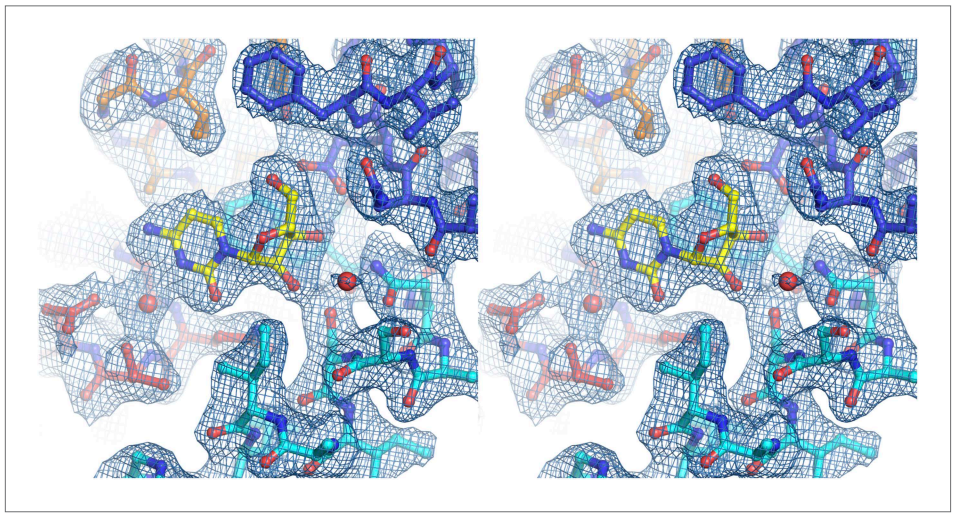

**Figure 4—figure supplement 1**. Electron density at the nucleoside-binding site of vcCNT-7C8C-cytidine. The nucleoside-binding site of vcCNT-7C8C bound to cytidine is shown in stereo in stick representation in the same orientation and colored as the structures in ***Figure 2***. Cytidine is yellow and the red spheres are water molecules. The resolution is 2.6 Å and density shown is from a $2F_o–F_c$ electron density map contoured at 1σ.

DOI: 10.7554/eLife.03604.018

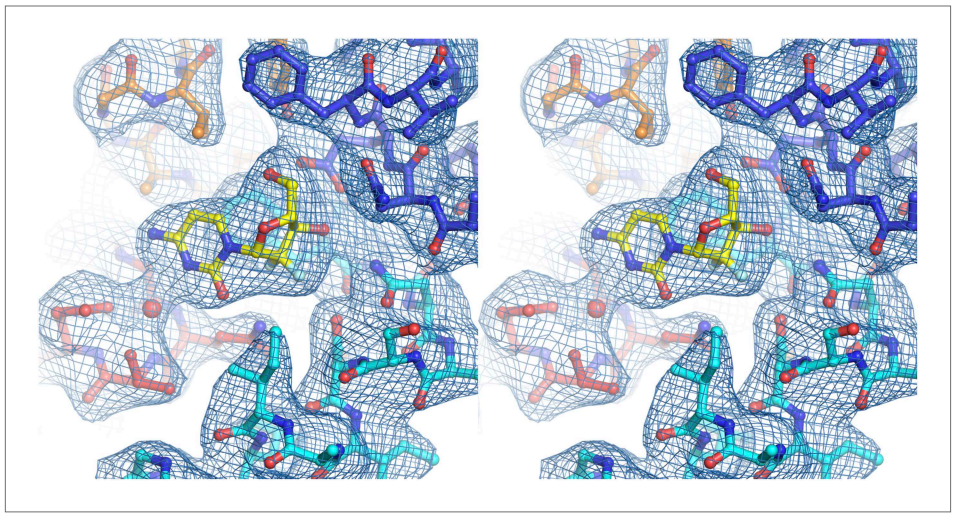

**Figure 4—figure supplement 2**. Electron density at the nucleoside-binding site of vcCNT-7C8C-gemcitabine. The nucleoside-binding site of vcCNT-7C8C bound to gemcitabine is shown in stereo in stick representation in the same orientation and colored as in ***Figure 4C***. Gemcitabine is yellow and the red sphere is a water molecule. The resolution is 2.9 Å and density shown is from a $2F_o–F_c$ electron density map contoured at 1σ.

DOI: 10.7554/eLife.03604.019

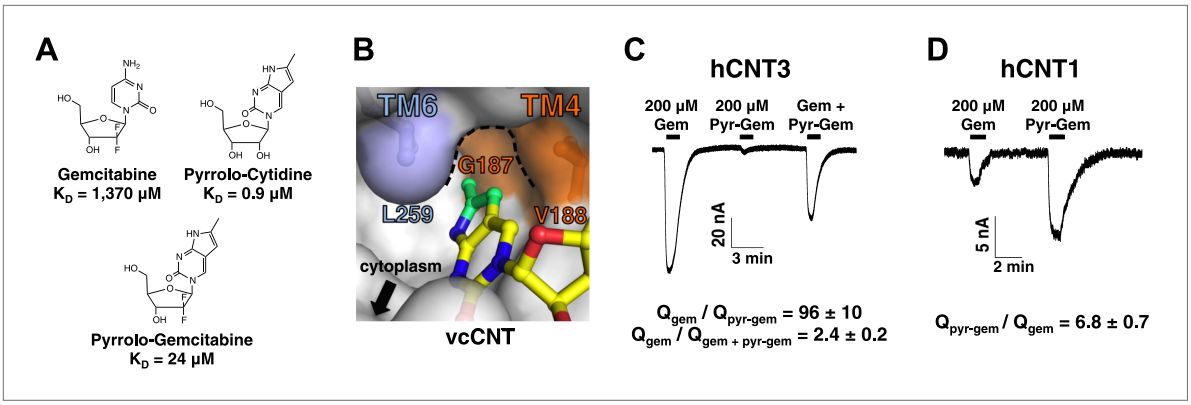


**Figure 5**. Design of pyrrolo-gemcitabine and its transportability by hCNTs. (**A**) Chemical structures and $K_D$s of gemcitabine and the pyrrolo-nucleosides. (**B**) The crystal structure of vcCNT-7C8C in complex with pyrrolo-cytidine is shown in surface representation with pyrrolo-cytidine shown in stick representation. The additional three carbons that comprise the methylpyrrole ring of pyrrolo-cytidine are colored green. The vcCNT-7C8C nucleo-pocket, formed mainly by G187 (TM4), V188 (TM4), and L259 (TM6), is delineated with a dotted line. The location of the cytoplasm, adjacent to the nucleo-pocket, is shown. For a stereo view of the electron density in the nucleoside-binding site, see ***Figure 5—figure supplement 1***. (**C**) hCNT3 transports gemcitabine but not pyrrolo-gemcitabine. $Na^+$ currents were elicited by the addition of nucleoside to *Xenopus* oocytes expressing hCNT3, and currents were measured by two-electrode voltage-clamp. An example current trace is shown. For each individual oocyte, the area under each current peak was measured to calculate total charge (Q) transported during application of nucleoside. The ratio of total charge co-transported with gemcitabine to that with pyrrolo-gemcitabine or gemcitabine total charge to gemcitabine + pyrrolo-gemcitabine total charge was calculated for each oocyte experiment (means ± SEM, n = 14 oocytes). For Gem + Pyr-Gem, 200 µM of each nucleoside was added simultaneously. (**D**) hCNT1 transports pyrrolo-gemcitabine better than gemcitabine. Same experiment as in **C** but hCNT1-expressing oocytes were used and the ratio of total charge for pyrrolo-gemcitabine to gemcitabine is shown (means ± SEM, n = 11 oocytes). Neither gemcitabine nor pyrrolo-gemcitabine elicited currents in water-injected oocytes (***Figure 5—figure supplement 2***) See ***Figure 5—source data 1*** for total charge source data.

DOI: 10.7554/eLife.03604.020

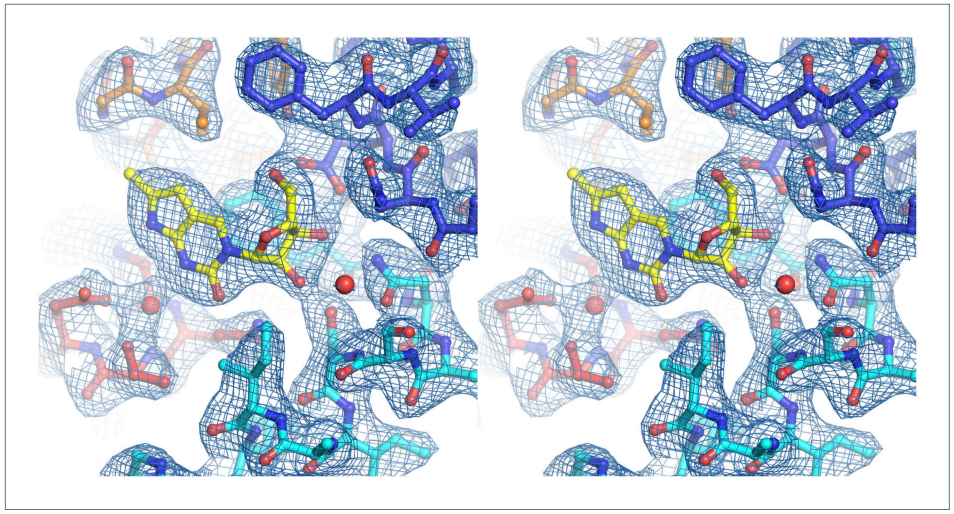

**Figure 5—figure supplement 1**. Electron density at the nucleoside-binding site of vcCNT-7C8C-pyrrolo-cytidine. The nucleoside-binding site of vcCNT-7C8C bound to pyrrolo-cytidine is shown in stereo in stick representation in the same orientation and colored as the structures in ***Figure 2***. Pyrrolo-cytidine is yellow, and the red spheres are water molecules. The resolution is 2.8 Å and density shown is from a $2F_o–F_c$ electron density map contoured at 1σ.

DOI: 10.7554/eLife.03604.022

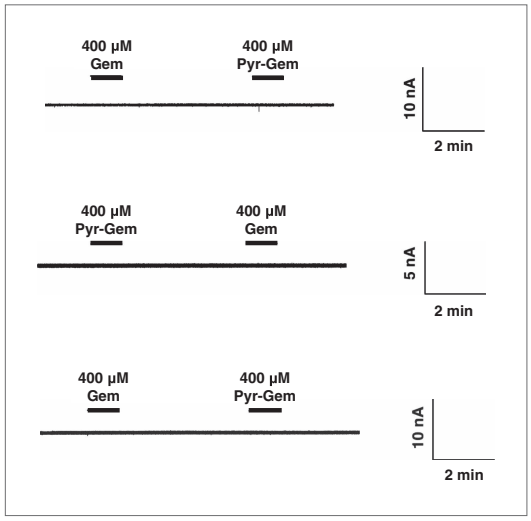


**Figure 5—figure supplement 2**. Water-injected oocytes do not respond to gemcitabine or pyrrolo-gemcitabine treatment. Current traces are shown for three different oocyte experiments. Experiments were performed in the same manner as those in 5C and 5D except water-injected oocytes were used.

DOI: 10.7554/eLife.03604.023

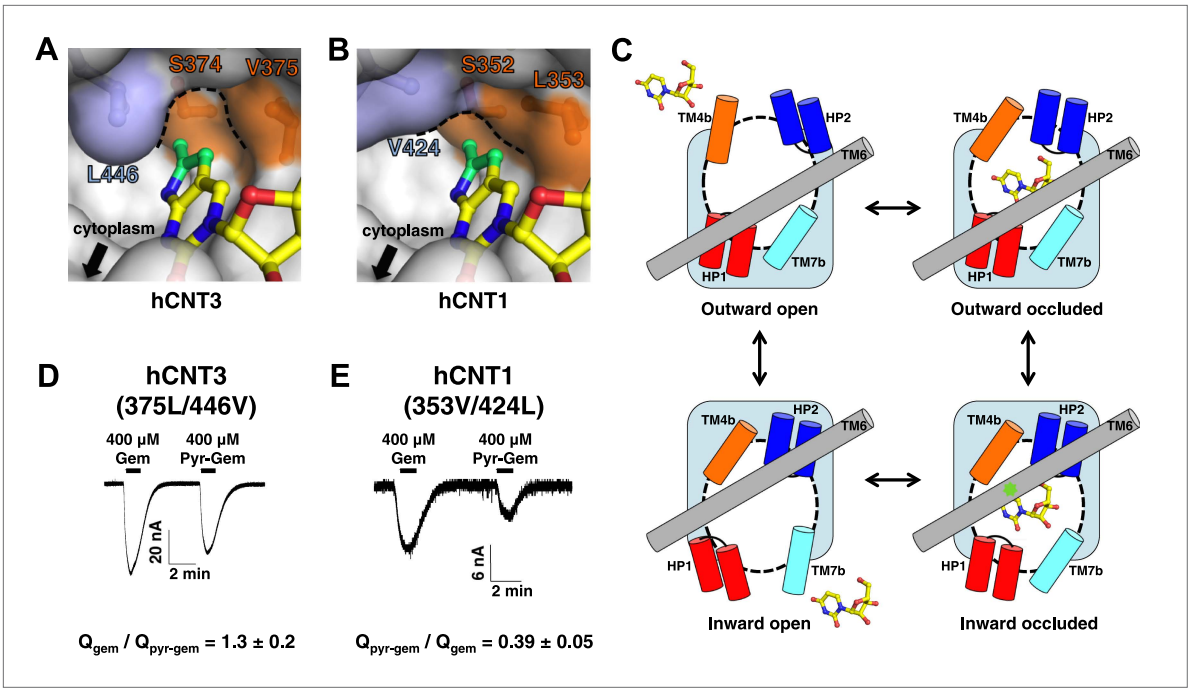


**Figure 6**. Structural basis of the subtype selectivity of pyrrolo-gemcitabine. (**A**) Model of hCNT3 nucleo-pocket. The structure of vcCNT-7C8C bound to pyrrolo-cytidine was used to generate a model of the hCNT3 nucleo-pocket by mutating the appropriate residues in PyMOL and selecting the rotamer that yielded the lowest amount of steric clash. (**B**) Model of hCNT1 nucleo-pocket. The model was generated in the same manner as **A**. Note that the methylpyrrole ring (green) will clash with the hCNT1 nucleo-pocket if it maintains the nucleoside-binding mode observed in the vcCNT structure. (**C**) Hypothetical alternating-access mechanism of vcCNT. A cartoon representation of the different conformational states along the transport cycle is depicted. The transport domain (including HP1, HP2, TM4b, and TM7b) and TM6 are shown as cylinders. Uridine is shown in stick representation. The nucleo-pocket in the inward-occluded conformation (bottom right) is located between TM6 and TM4 and is marked with a green star. The inward-occluded conformation is derived from the crystal structures of vcCNT. All other conformations are purely hypothetical. The transition between inward- and outward-facing conformations has been proposed to be achieved by a rigid-body movement of the transport domain across TM6 (***Johnson et al., 2012***). Extracellular and intracellular gating likely involves slight rearrangements of HP2/TM4b and HP1/TM7b, respectively. (**D**) hCNT3 (375L/446V) is capable of transporting both gemcitabine and pyrrolo-gemcitabine. Same experiment as ***Figure 5C,D*** but hCNT3 (375L/446V)-expressing oocytes were used and the ratio of total charge (Q) co-transported with gemcitabine to pyrrolo-gemcitabine is shown (means ± SEM, n = 11 oocytes). (**E**) hCNT1 (353V/424L) transports pyrrolo-gemcitabine less efficiently than gemcitabine (means ± SEM, n = 8 oocytes). Note that a higher nucleoside concentration was needed for **D** and **E** than the wild-type experiments due to lower transporter activity and/or expression. See ***Figure 6—source data 1*** for total charge source data.

DOI: 10.7554/eLife.03604.024